Chinese Journal of Chemical Engineering 90 (2026) 272–282

Contents lists available at ScienceDirect

Chinese Journal of Chemical Engineering

journal homepage: www.elsevier.com/locate/CJChE

Full Length Article

Isobaric vapor–liquid equilibrium for the binary system of methyl propionate and methyl methacrylate at 90.0, 75.0, 60.0, 45.0 and 30.0 kPa

Junping Zhang [1, 2], Songsong Chen [2, 3], Shasha Cao [2], Chunshan Li [2, 3], Hui Zhao [1], Xiangping Zhang [2, *], Chaohe Yang [1, *]

[1] State Key Laboratory of Heavy Oil Processing, China University of Petroleum, Qingdao 266580, China
[2] Beijing Key Laboratory of Solid State Battery and Energy Storage Process, State Key Laboratory of Mesoscience and Engineering, Institute of Process Engineering, Chinese Academy of Sciences, Beijing 100190, China
[3] School of Chemical Engineering, University of Chinese Academy of Sciences, Beijing 100049, China

ARTICLE INFO

Article history:
Received 16 June 2025
Received in revised form
11 September 2025
Accepted 12 September 2025
Available online 30 October 2025

Keywords:
Vapor–liquid equilibria
Thermodynamic model
Simulation
Separation

ABSTRACT

Based on the requirements for the separation process of methyl methacrylate (MMA) production, thermodynamic behavior related to MMA was systematically studied. Isobaric vapor–liquid equilibrium (VLE) data for the binary system of methyl propionate and MMA at 90.0, 75.0, 60.0, 45.0 and 30.0 kPa were measured by a modified Rose equilibrium still at temperatures ranging from 319.4 K to 372.2 K. The accuracy of the VLE data is validated using the Herington area test and the Fredenslund point test. The experimental results were correlated using the non-random two liquid, Wilson and universal quasi-chemical (UNIQUAC) thermodynamic models. The binary interaction parameters for each model were determined by employing a maximum likelihood objective function for optimization. All three models exhibited a high degree of correlation with the experimental data. The results provide valuable insights for the design and optimization of the separation process in MMA production. The results show that the model with fitted parameters has a reduction of more than 38% in total equipment investment cost compared to the UNIFAC model, indicating that the correction of VLE parameters has practical application value in guiding process design and production.

1. Introduction

Methyl methacrylate (MMA), a key unsaturated ester monomer for producing poly(methyl methacrylate) (PMMA), is widely used in coatings, medical, construction and electronics industries [1–3]. Growing demand for MMA and stricter environmental regulations, have driven manufacturers to develop eco-friendly MMA synthesis technologies. Among these methods, the aldol condensation of methyl propionate (MP) with formaldehyde (FA) for MMA production has attracted significant research interest [4–6]. In recent years, researchers have conducted extensive research on catalyst design and evaluation. However, separation and purification of crude MMA remain critical industrial challenges.

MMA is prone to polymerization at elevated temperatures due to the presence of double bonds and carbonyl groups [7]. Consequently, the separation of MMA is typically operated under vacuum distillation [8]. Accurate phase equilibrium data are crucial for the research of distillation separation processes. To obtain a high purity MMA product, accurate vapor–liquid equilibrium (VLE) data for MP–MMA components are indispensable for the design and optimization of the separation process. While the phase equilibrium of related binary mixtures, such as methanol (MeOH)–MP [9–12] and MeOH–MMA [9,13], has been extensively studied. VLE data for MP–MMA at atmospheric pressure have also been reported [9]. However, there is a lack of reported data for the MP–MMA system under vacuum pressure conditions.

In this study, the VLE data for the binary system (MP–MMA) were measured at pressures of 90.0, 75.0, 60.0, 45.0 and 30.0 kPa. The thermodynamic consistency of the VLE data was validated using the Herington area test and Fredenslund point test [14–16].

* Corresponding authors.
E-mail addresses: xpzhang@ipe.ac.cn (X. Zhang), yangch@upc.edu.cn (C. Yang).

https://doi.org/10.1016/j.cjche.2025.09.019

Moreover, the isobaric VLE data were modeled using the non-random two liquid (NRTL), Wilson and universal quasi-chemical (UNIQUAC) models, and the corresponding parameters of MP and MMA were obtained, respectively.

2. Experimental

2.1. Materials

MeOH, MP, and MMA were purchased from Shanghai Aladdin Co., Ltd. (China) without further treatment. MeOH and MP were primarily employed to assess the functionality and accuracy of the experimental apparatus. The purity of reagents was verified by GC and mass fractions were higher than 99.0%, the uncertainties of measured density are calculated using the report methods [17] and listed in the Supplementary Material document. The basic characteristics and structural parameters of the reagents used in this study are listed in Table 1.

2.2. VLE apparatus and experimental procedure

Isobaric VLE data for MP and MMA were obtained using a modified Rose equilibrium still equipped with a vacuum control system [23,24] as shown in Fig. 1. The apparatus consisted of several components, including a heating rod, liquid and gas phase sampling ports, a balance chamber, a precision mercury thermometer and a spiral condenser. The system was heated with a variable-voltage regulator (0–220 V, 12 A) and a heating rod. The variable-voltage regulator operates at a constant current of 12 A, allowing the heating power to be adjusted by varying the output voltage. The vacuum was controlled by vacuum pump system (KNF SC-950, Germany), which was connected to the still *via* a rubber tube to maintain a constant pressure and form an isobaric vacuum environment with the system pressure accuracy of 0.1 kPa. The pressure and temperature were monitored with a digital pressure gauge and a precision mercury thermometer, both of which had passed the precision test by Beijing Institute of Metrology, China. The measured pressure and temperature indicator were read by taking the average of three readings to determine the stable values as the determined value. Experiments were performed at 90.0, 75.0, 60.0, 45.0, and 30.0 kPa, respectively. For each test, 40 ml of the mixture was introduced into the still and gradually heated. As vapor formed, the liquid and gas phases were continuously circulated to ensure intimate contact. The equilibrium temperature of the mixture was maintained for 1 h, with the temperature strictly controlled by the mercury thermometer to ensure stability within ±0.1 K over the course of an hour, signifying that vapor–liquid equilibrium had been achieved. Once the system reached equilibrium, the measured pressure and temperature were recorded every 5 min, with the average value of the three readings taken as the final determined value. Samples from both phases were subsequently collected using a syringe and subjected to GC analysis. To avoid air ingress during the sampling process, the fully covered vacuum-resistant and chemically stable Viton sealing gaskets for both the liquid and vapor phase sampling ports were selected. On the other hand, a syringe with the size of 0.5 mm × 30 mm was chosen to extract gas and liquid phase samples, and could contain the vacuum pressure remains unchanged during the sampling process.

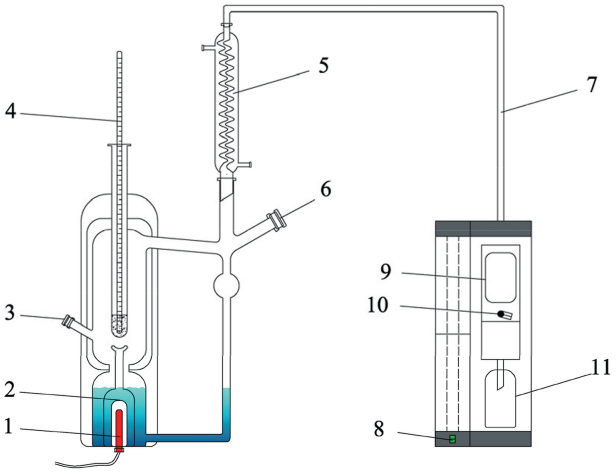

Fig. 1. Schematic of the VLE apparatus: (1) heating rod, (2) vapor–liquid phase equilibrium chamber, (3) liquid phase sampling port, (4) precision mercury thermometer, (5) condensing pipe, (6) vapor phase condensate sampling port, (7) rubber tube, (8) KNF diaphragm pump power switch, (9) pressure indicator, (10) pressure regulating knob, (11) liquid collecting bottle.

2.3. Sample analysis

The condensed vapor and liquid phase compositions were analyzed using an offline gas chromatograph (Shimadzu GC-2030, Japan), which was equipped with a flame ionization detector (FID) and a capillary column (SH-RTX-5, 30.0 m × 0.25 mm × 0.25 μm). Pure nitrogen gas (99.999%) (mass) was used as the carrier gas. The volume of sample injected each time was 0.2 μl. The operating conditions were as follows: The column temperature was set at 308.15 K and maintained for 3 min, then increased from 308.15 K to

Table 1
Basic characteristics and structural parameters of the reagents.

Component *i*	CAS	MW /g·mol^{-1}	Density ① /g·cm^{-3}		V_m/cm^3·mol^{-1}	*r*	*q*	Purity/% (mass)		Supplier
			Exp.	Lit.				GC	Suppler	
Methanol (MeOH)	67-56-1	32.042	0.786722	0.7864 ②	41.5	1.4311⑥	1.432 ⑥	>99.9	99.9	Shanghai Aladdin
Methyl propionate (MP)	554-12-1	88.105	0.909145	0.9091 ③	96.3	3.479 ⑥	3.116 ⑥	>99.0	99.0	Co., Ltd., China
Methyl methacrylate (MMA) ④	80-62-6	100.12	0.937652	0.9376 ⑤	106.8	3.922 ⑦	3.564 ⑦	>99.0	99.0	

Where, *r* and *q* are the UNIQUAC structural parameters.
① At 298.15 K, $u(\rho)_{MP} = 0.000612$ g·cm^{-3}, $u(\rho)_{MMA} = 0.000755$ g·cm^{-3}.
② From literature [18].
③ From literature [19].
④ Contains 0.03 kg·m^{-3} DMBP as stabilizer.
⑤ From literature [20].
⑥ From literature [21].
⑦ From literature [22].

503.15 K with a rate of 10 K·min^{-1}, and remained at 503.15 K for 7.5 min. Both the detector and injector were maintained at 503.15 K. Quantification was performed using the external standard method, which was used to detect the composition of each component, with each sample analyzed a minimum of three times to confirm accuracy. The GC calibration curve and fitted parameters are shown in Fig. S5 and Eq. (S1). The temperature uncertainty is 0.18 K, and the pressure uncertainty is 0.18 kPa. The standard uncertainty of vapor and liquid phase compositions has been calculated, and the result is 0.001 as shown in Table S4. The calculation process was supplemented in Supplementary Material as listed in Tables S2–S4.

3. Results and Discussion

3.1. Validation of the apparatus

The reliability of the VLE apparatus was tested using the well-documented binary system of MeOH and MP at 100.0 kPa, and the test results were provided in the Table S1 [12]. The results showed that the deviation was within 2% as illustrated in Figs. S3–S4, thereby confirming the dependability of the device and the experimental methodology employed.

The saturated vapor pressures of MP (319.4 K $\leq T \leq$ 351.8 K) and MMA (337.9 K $\leq T \leq$ 372.2 K) were determined using the equilibrium still apparatus, and the results were listed in Table 2. The vapor pressures P^* of each pure component were calculated employing the Antoine equation [25] in this work, described by Eq. (1), where P_i^* is the saturated vapor pressure of component i (in kPa), T is the equilibrium temperature (in K), A, B and C are Antoine coefficients. Temperature range for the equation constants of MP and MMA are listed in Table 3 respectively.

$$\lg P^* = A - \frac{B}{C+T} \tag{1}$$

To assess the consistency and accuracy of the experimental data, these results were analyzed and compared with previous research [9,21,26,27]. The absolute deviations of pressure compared to the literature data were depicted in Figs. S1 and S2. For the temperature range studied, Shi's equation [9] and Ríos *et al.* [19] were selected to estimate the saturated vapor pressures of MP and MMA within this temperature interval. The results indicated that the estimates from Shi's equation [9] are lower than the experimental values, while those from Ríos *et al.* [19] are higher. As shown in Fig. 2, the average relative deviations of vapor pressure for MP and MMA are around with 1.0% to 1.3%, which have been shown much reliable and applicable as compared to the reference [9]. The vapor pressure experimental data have been employed to the Antoine equation parameters fitting and listed in Table 3.

Table 2
Vapor pressure data for MP and MMA ①.

P^*/kPa	T_{MP}/K	P^*/kPa	T_{MMA}/K
100.0	351.8	100.0	372.2
90.0	348.6	90.0	368.9
80.0	345.1	80.0	365.2
70.0	341.3	70.0	361.2
60.0	337.0	60.0	356.7
50.0	332.2	50.0	351.6
40.0	326.4	40.0	345.5
30.0	319.4	30.0	337.9

① The standard uncertainty of the system (u) of T and P were $u(T) = 0.18$ K, $u(P) = 0.18$ kPa.

Table 3
Antoine equation constants of MP and MMA.

Component i	A	B	C	Temperature range/K	R^2
MP	6.088	1169.8	−65.63	319.4–351.8	99.998%
MMA	6.557	1516.2	−39.46	337.9–372.2	99.997%

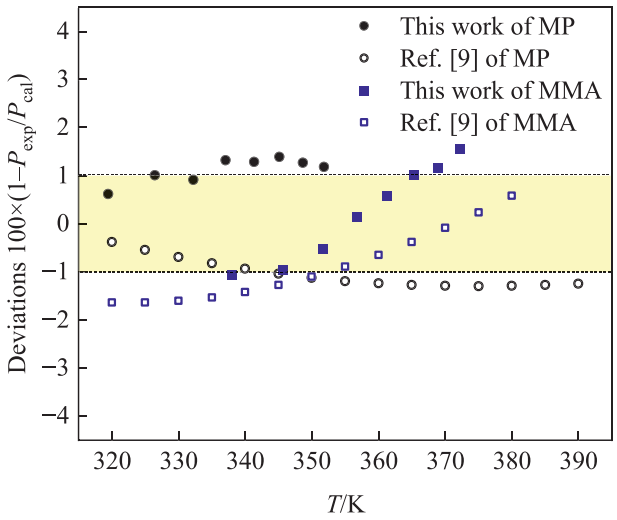

Fig. 2. The absolute deviations of pressure of MP and MMA between experimental data and calculated data by DIPPR parameters, where the "P_{cal}" were calculated with DIPPR database, the black points "●" and blue points "■"are experimental data of this work, "○" and "□" are the data come from Ref. [9].

3.2. VLE data and calculation

The VLE experimental data for the MP–MMA system at various pressures are presented in Table 4. Upon reaching equilibrium, the thermodynamic relationship between the vapor and liquid phases can be described by Eq. (2) [28].

$$Py_i\hat{\phi}_i^{v} = \gamma_i x_i P_i^* \phi_i^* \exp\int_{P_i^*}^{P} \frac{V_i^L}{RT}\mathrm{d}P \tag{2}$$

where P (Pa) is the total pressure of the VLE system, P_i^* (Pa) is the saturated vapor pressure of pure component i at temperature T (K), y_i is the mole fraction of component i in the vapor phase, x_i is the mole fraction of component i in the liquid phase, γ_i is the activity coefficient of component i, $\hat{\phi}_i^{v}$ and ϕ_i^* are the fugacity coefficients of component i in the mixture vapor phase and in the pure state respectively, V_i^L is the molar volume of component i, and R is the gas constant.

The vapor phase behavior can be approximated as ideal under conditions where the experimental pressures are below 101.3 kPa. In such cases, the fugacity coefficient for the vapor phase is approximately 1. Additionally, when the contribution of the liquid-phase molar volume to the integral term is considered negligible, the Poynting factor is also approximately 1. Consequently, the VLE relationship can be simplified by Eq. (3) [28]. Here, the saturated pressure P_i^* of each component can be calculated from the Antoine equation with the constants specified in Table 3. The activity coefficients γ_i are calculated using Eq. (3) and listed in Table 4.

Table 4
VLE experimental data for MP (1) and MMA (2) at 90.0, 75.0, 60.0, 45.0, and 30.0 kPa [①].

P/kPa	T/K	x_1	y_1	γ_1	γ_2	α_{12}
90.0	348.6	1.000	1.000	1.002		–
	349.1	0.957	0.972	1.001	1.276	1.569
	349.9	0.904	0.939	0.996	1.223	1.626
	351.6	0.798	0.873	0.992	1.134	1.736
	353.2	0.695	0.807	1.000	1.075	1.838
	355.1	0.592	0.737	1.008	1.024	1.934
	357.1	0.493	0.663	1.020	0.987	2.021
	358.7	0.401	0.584	1.052	0.975	2.097
	361.3	0.290	0.471	1.082	0.957	2.183
	363.7	0.197	0.355	1.117	0.952	2.250
	366.3	0.105	0.213	1.163	0.957	2.312
	367.6	0.058	0.126	1.196	0.968	2.342
	368.9	0.000	0.000		0.997	–
75.0	343.4	1.000	1.000	0.998		–
	344.1	0.957	0.972	0.990	1.264	1.589
	344.7	0.904	0.939	0.991	1.223	1.642
	346.4	0.798	0.874	0.985	1.134	1.752
	348.2	0.693	0.807	0.986	1.067	1.853
	349.8	0.597	0.742	0.997	1.025	1.941
	352.0	0.490	0.662	1.007	0.981	2.036
	353.8	0.399	0.584	1.030	0.960	2.116
	356.0	0.293	0.475	1.066	0.951	2.188
	358.5	0.191	0.350	1.106	0.948	2.280
	360.8	0.100	0.207	1.157	0.962	2.350
	362.1	0.054	0.119	1.189	0.972	2.391
	363.4	0.000	0.000		0.998	–
60.0	337.0	1.000	1.000	1.004		–
	338.1	0.958	0.974	0.981	1.230	1.646
	339.1	0.902	0.940	0.969	1.171	1.704
	340.4	0.798	0.877	0.976	1.106	1.809
	342.1	0.689	0.809	0.981	1.047	1.912
	343.5	0.601	0.750	0.993	1.014	1.991
	345.5	0.493	0.669	1.008	0.979	2.081
	347.5	0.390	0.580	1.032	0.959	2.161
	349.7	0.283	0.469	1.067	0.952	2.236
	351.9	0.190	0.350	1.103	0.953	2.297
	354.2	0.097	0.201	1.156	0.968	2.353
	355.3	0.055	0.122	1.184	0.978	2.377
	356.7	0.000	0.000		0.999	–
45.0	329.5	1.000	1.000	0.998		–
	330.2	0.958	0.975	0.989	1.216	1.717
	330.9	0.903	0.945	0.988	1.173	1.865
	332.3	0.798	0.883	0.991	1.103	1.914
	333.8	0.692	0.814	1.001	1.051	1.948
	335.6	0.603	0.754	0.998	1.001	2.023
	337.6	0.498	0.672	1.007	0.969	2.066
	339.3	0.395	0.582	1.038	0.961	2.132
	341.5	0.292	0.471	1.065	0.951	2.159
	343.9	0.195	0.351	1.092	0.947	2.230
	346.2	0.097	0.202	1.147	0.966	2.354
	347.5	0.055	0.123	1.166	0.970	2.416
	348.8	0.000	0.000		0.996	–
30.0	319.4	1.000	1.000	0.999		–
	319.7	0.969	0.983	0.999	1.195	1.817
	320.5	0.904	0.946	0.999	1.162	1.864
	322.1	0.773	0.870	1.002	1.101	1.966
	323.5	0.683	0.816	1.008	1.055	2.054
	325.2	0.575	0.743	1.017	1.020	2.134
	326.6	0.510	0.695	1.015	0.990	2.187
	328.6	0.382	0.587	1.056	0.977	2.293
	330.6	0.276	0.472	1.086	0.977	2.342
	333.1	0.177	0.340	1.114	0.974	2.393
	335.5	0.091	0.197	1.138	0.971	2.437
	337.0	0.048	0.111	1.149	0.968	2.456
	337.9	0.000	0.000		1.001	–

[①] The standard uncertainty of the system (u) of T, p, x, and y were $u(T) = 0.18$ K, $u(P) = 0.18$ kPa, and $u(x) = u(y) = 0.001$.

$$Py_i = P_i^* \gamma_i x_i \tag{3}$$

The relative volatility α_{12} of MP with regard to MMA can be calculated by Eq. (4) [29] and shown in Fig. 3.

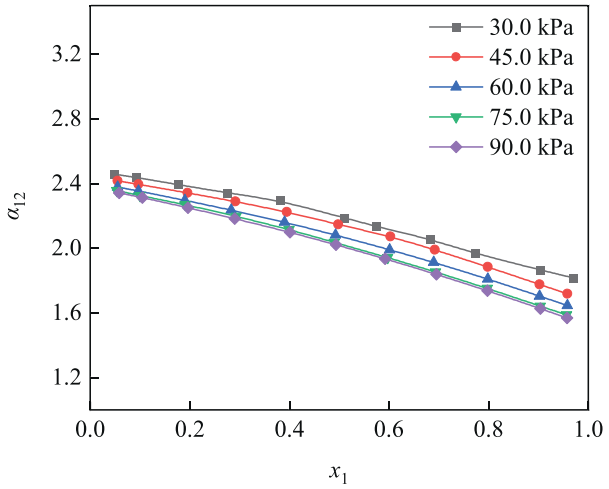

Fig. 3. Relative volatility of the experimental liquid mole fraction (x_1) for MP (1) + MMA (2) systems at 90.0, 75.0, 60.0, 45.0, and 30.0 kPa.

$$\alpha_{12} = \left(\frac{y_1}{x_1}\right) \Big/ \left(\frac{y_2}{x_2}\right) \tag{4}$$

The analysis of VLE data was further enhanced by examining the relative volatilities of the two components. It was observed that the relative volatility between MP and MMA increases with decreasing pressure, demonstrating a notable positive correlation with reduced system pressure. For example, at a mole fraction of 0.2 for MP, the α_{12} value at 30.0 kPa is higher than that at 90.0 kPa, indicating that operating at lower pressures can be beneficial for the separation of these components. The results also show that as the mole fraction of x_1 increases, the relative volatility α_{12} shows a decreasing trend. This insight is crucial for optimizing the distillation process in industrial applications to obtain high purity MMA.

3.3. Thermodynamic correlations

In this investigation, the classical NRTL, Wilson and UNIQUAC models were employed to correlate the VLE experimental data. For the NRTL model, the non-randomness parameter (α) was set at 0.3 [30] in accordance with the conventional values used for binary mixtures.

The NRTL equation model of two components mixture is given as Eqs. (5) and (6) [31]:

$$\ln \gamma_i = x_j^2 \left[\tau_{ji} \left(\frac{G_{ji}}{x_i + x_j G_{ji}} \right)^2 + \frac{G_{ij}\tau_{ij}}{\left(x_j + x_i G_{ij}\right)^2} \right] \tag{5}$$

where,

$$G_{ij} = \exp\left(-\alpha \tau_{ij}\right) \quad \tau_{ij} = a_{ij} + \frac{b_{ij}}{T} \tag{6}$$

Wilson equation model is listed as Eqs. (7) and (8) [32]:

$$\ln \gamma_i = -\ln\left(x_i + \Lambda_{ij} x_j\right) + x_j \left(\frac{\Lambda_{ij}}{x_i + \Lambda_{ij} x_j} - \frac{\Lambda_{ji}}{x_j + \Lambda_{ji} x_i} \right) \tag{7}$$

where,

$$\ln \Lambda_{ij} = a_{ij} + \frac{b_{ij}}{T}\ a_{ij} = \ln \frac{V_j}{V_i}\ b_{ij} = \frac{-\left(g_{ij} - g_{ii}\right)}{R} \tag{8}$$

UNIQUAC equation model is calculated using the following Eqs. (9)–(11) [33]:

$$ln\ \gamma_i = ln\frac{\phi_i}{x_i} + \frac{z}{2}q_i\ ln\frac{\theta_i}{\phi_i} + l_i - \frac{\phi_i}{x_i}\sum_j\left(x_j l_j\right) - q_1\ ln\left[\sum_k(\theta_k\tau_{ki})\right] + q_i - q_i\sum_j\frac{\theta_j\tau_{ij}}{\sum_k\theta_k\tau_{ki}} \tag{9}$$

where,

$$\theta_i = \frac{x_i q_i}{\sum_j x_j q_j}\ \phi_i = \frac{x_i r_i}{\sum_j x_j r_j} \tag{10}$$

$$l_i = \frac{z}{2}(r_i - q_i) + 1 - r_i\ \tau_{ij} = \exp\left(a_{ij} + \frac{b_{ij}}{T}\right) \tag{11}$$

The objective function (OF) for parameter estimation is the maximum likelihood target function, as stated in Eq. (12) [34]. This function is comprehensive, considering all measured variables concurrently, thereby ensuring that the derived parameters for the models are robustly justified.

$$\mathrm{OF} = \sum_{i=1}^{N}\left|\left(\frac{T_i^{\exp} - T_i^{\mathrm{cal}}}{\sigma_T}\right)^2 + \left(\frac{P_i^{\exp} - P_i^{\mathrm{cal}}}{\sigma_p}\right)^2 + \left(\frac{x_i^{\exp} - x_i^{\mathrm{cal}}}{\sigma_x}\right)^2 + \left(\frac{y_i^{\exp} - y_i^{\mathrm{cal}}}{\sigma_y}\right)^2\right| \tag{12}$$

The binary interaction parameters deduced for each activity coefficient model are detailed in Table 5. The evaluation of these models' accuracy in fitting the experimental data is quantified by calculating the average absolute deviation (AAD) and the root mean square deviation (RMSD). AAD reflects the accuracy of the calculated data in relation to the experimental data, while RMSD measures the spread of these data points. The deviation encountered in the regression analysis using NRTL, Wilson and UNIQUAC models are presented in Table 6 for the binary system (MP–MMA). The reported AAD (T) values are less than 1.1 K and AAD (y_1) values are less than 0.008, RMSD values (T) are less than 1.2 K and RMSD (y_1) values are less than 0.011. The RMSD (y_1) value of the UNIQUAC model is higher than the NRTL and Wilson models, showing that the NRTL and Wilson models have a relatively low deviation from the experimental values.

The experimental data and the values predicted by the three activity coefficient models exhibit a notable level of agreement. This consistency is visually confirmed in the T–x–y diagram of Fig. 4, which shows that the fitting degree of UNIQUAC is higher, indicating that the UNIQUAC thermodynamic method is more appropriate for simulating the MMA separation process. In the phase diagram, the VLE lines for the two components are relatively close, indicating that the substances have similar volatilities, which presents a challenge for separation. To achieve high-purity products through distillation, a larger number of theoretical plates and a higher reflux ratio are required. This graphical representation not only highlights the effectiveness of the models but also serves to validate the thermodynamic consistency and reliability of the derived parameters.

Table 5
Binary interaction parameters of NRTL, Wilson and UNIQUAC activity coefficient models for the binary system MP–MMA.

Model	a_{12}	a_{21}	b_{12}/K	b_{21}/K
NRTL①	−0.048	−0.145	99.709	50.072
Wilson②	0.103	−0.103	32.696	−137.59
UNIQUAC③	0.572	−0.447	−336.400	260.100

① NRTL, $\tau_{ij} = a_{ij} + b_{ij}/T$, $\alpha = 0.3$.
② Wilson, $\ln \Lambda_{ij} = a_{ij} + b_{ij}/\mathrm{T}$.
③ UNIQUAC, $\tau_{ij} = \exp(a_{ij} + b_{ij}/T)$.

3.4. Thermodynamic consistency test

In the present study, the thermodynamic consistency of the VLE experimental data was validated and assessed by using the Herington area test and the Fredenslund test [16,35], ensuring the reliability of experimental findings.

The thermodynamic consistency of the VLE data was first assessed *via* the Herington method, which is based on the Gibbs–Duhem equation, and expressed by Eq. (13) [35]. Under isobaric conditions, the left side and the initial term on the right side of Eq. (13) are equal to 0. In practice, plotting the natural logarithm of the activity coefficient ratio $\ln(\gamma_1/\gamma_2)$ against the mole fraction of component x_1, allows for the calculation of the areas above (A^+) and below (A^-) the x-axis. The net area represented by D can be calculated by Eq. (14) [9,25]. Furthermore, the influence of temperature variation is quantified by the variable J in Eq. (15) [9,16], which takes into consideration the $T_{\max}$ and $T_{\min}$ temperatures recorded within the experimental system. If the absolute difference of $|D–J|$ is less than 10, the data are considered consistent, otherwise, the experimental data should be rejected [9,16]. As the results listed in Table 7, VLE experimental data have successfully passed the Herington test.

$$\int_{x_1=0}^{x_1=1}\ln\frac{\gamma_1}{\gamma_2}\mathrm{d}x_1 = -\int_{P(x_1=0)}^{P(x_1=1)}\frac{V^E}{RT}\mathrm{dP} + \int_{T(x_1=0)}^{T(x_1=1)}\frac{H^E}{RT^2}\mathrm{d}T \tag{13}$$

$$D = 100\frac{\left|\int_0^1\ln\frac{\gamma_1}{\gamma_2}\right|}{\int_0^1\left|\ln\frac{\gamma_1}{\gamma_2}\right|} = 100\frac{||A^+| - |A^-||}{|A^+| + |A^-|} \tag{14}$$

$$J = 150 \times \frac{T_{\max} - T_{\min}}{T_{\min}} \tag{15}$$

The Fredenslund method [16,35] as illustrated by Eq. (16) [24] measures thermodynamic consistency by calculating the mean relative deviation. The mean relative deviation $\Delta|y|$ is defined as the average of the absolute deviations between experimental data and calculate value, exp is the experimental measurement data, cal is the model calculated result, and N is the number of experimental data. For this method, the VLE data are deemed to pass the point-by-point test when the average absolute deviation of the experimental data and the calculated data for the vapor phase mole fraction $\Delta|y|$ is less than 0.01 [36]. The Results of Fredenslund consistency tests at various pressures are summarized in Table 8, indicating that the calculations passed the Fredenslund test.

$$\Delta|y| = \frac{1}{N}\sum_{i=1}^{N}\left|y_i^{\exp} - y_i^{\mathrm{cal}}\right| \tag{16}$$

Experimental and calculated values of γ_i for the MP–MMA binary system at various pressures are shown in Fig. 5. The results

Table 6
AAD and RMSD of T and y_1 for the binary system ①.

Pressure/kPa			30.0	45.0	60.0	75.0	90.0	Max.	Min.	Ave.
AAD ②	UNIQUAC	T/K	0.6	0.6	0.6	0.5	0.3	0.6	0.3	0.52
	Wilson		0.7	1.0	1.1	1.0	0.8	1.1	0.7	0.92
	NRTL		0.6	1.0	1.1	1.0	0.8	1.1	0.6	0.90
	UNIQUAC	y	0.008	0.008	0.008	0.008	0.008	0.008	0.008	0.008
	Wilson		0.002	0.002	0.001	0.001	0.002	0.002	0.001	0.002
	NRTL		0.004	0.003	0.001	0.001	0.003	0.004	0.001	0.002
RMSD ③	UNIQUAC	T/K	0.6	0.7	0.7	0.6	0.4	0.7	0.4	0.60
	Wilson		0.8	1.1	1.2	1.2	1.0	1.2	0.8	1.06
	NRTL		0.7	1.1	1.2	1.2	1.0	1.2	0.7	1.04
	UNIQUAC	y	0.011	0.011	0.010	0.010	0.011	0.011	0.01	0.011
	Wilson		0.003	0.002	0.001	0.002	0.003	0.003	0.001	0.002
	NRTL		0.006	0.004	0.002	0.002	0.003	0.006	0.002	0.003

① $u(T) = 0.18$ K, $u(P) = 0.18$ kPa, and $u(x) = u(y) = 0.001$.

② AAD $= \frac{\sum_{i=1}^{N} |\theta_{i,\mathrm{exp}} - \theta_{i,\mathrm{cal}}|}{N}$, where N is the experimental data number and θ is parameters (T and y in this case).

③ RMSD $= \left(\sum_{i=1}^{N} \frac{(\theta_{i,\mathrm{exp}} - \theta_{i,\mathrm{cal}})^2}{N} \right)^{0.5}$, where N is the experimental data number and θ is parameters (T and y in this case).

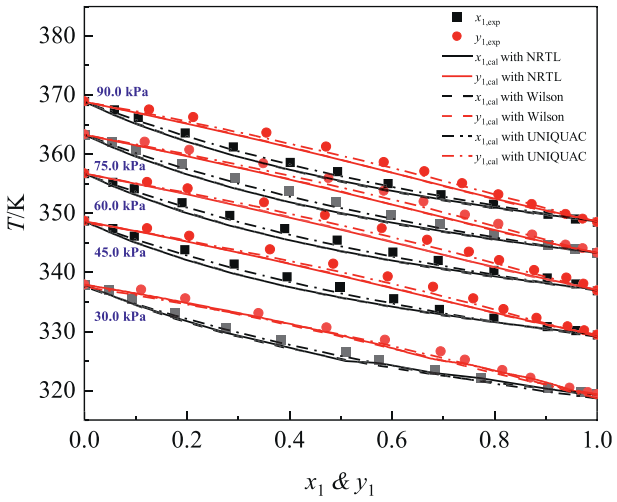

Fig. 4. T–x–y diagram for the binary system MP (1)–MMA (2) fit with the NRTL/Wilson/UNIQUAC models at 90.0, 75.0, 60.0, 45.0 and 30.0 kPa. The samples "●" and "■" refer to mole fraction of MP in vapor and liquid obtained from experiments respectively.

indicate that the trend lines generated by three thermodynamic methods align well with the experimental data. Among these, the Wilson model exhibits the smallest deviation, suggesting it provides the best fit for the dataset under investigation.

The Fredenslund test is considered essential but not robust enough to guarantee uniformity [16]. It relies on global statistical data, ignoring local discrepancies. Consequently, it is typically paired with an analysis of the residual distribution which examines the distribution of discrepancies in equilibrium temperature. These residuals of the equilibrium temperature (ΔT) and vapor composition (Δy) are shown in Fig. 6, which can be defined by Eqs. (17) and (18) [16]. This comprehensive evaluation not only assures the accuracy of the VLE data but also supports the reliability of the thermodynamic models used in this study, particularly demonstrating the effectiveness of the three models for this specific binary system. The findings indicate that the deviations between the experimental values and the estimated values obtained through the three models are exceptionally minor, highlighting a strong correlation between the experimental and estimated data. Specifically, in terms of the vapor composition (Δy), the average deviation using the NRTL and Wilson model methods are less than 0.003, signifying superior performance of the NRTL and Wilson model in estimating vapor compositions. Concerning the equilibrium temperature of the MP (1) + MMA (2) binary system, the absolute average deviation calculated using the NRTL and Wilson models are within 1.9 K. The UNIQUAC model, on the other hand, exhibits an even smaller deviation of less than 1.0 K. However, it is noteworthy that the UNIQUAC method presents a relatively large deviation in predicting vapor composition, with a discrepancy of approximately 0.02 when the liquid mole fraction for MP of 0.2. This observation suggests that while the UNIQUAC model is accurate for equilibrium temperature predictions, it may be less precise for vapor composition estimations in this specific binary system.

$$\Delta T = T_{\mathrm{exp}} - T_{\mathrm{cal}} \tag{17}$$

$$\Delta y = y_{\mathrm{exp}} - y_{\mathrm{cal}} \tag{18}$$

Table 7
Results of Herington consistency tests.

Pressure/kPa	D	J	$\lvert D-J \rvert$	Area test results
90.0	10.4	8.8	1.6	Passed
75.0	4.3	8.7	4.4	Passed
60.0	8.5	8.8	0.3	Passed
45.0	17.3	8.8	8.5	Passed
30.0	16.0	8.7	7.3	Passed

3.5. Process simulation

The fitted binary interaction parameters were applied to the separation calculation for the MP–MMA system. To compare the

Table 8
Results of Fredenslund consistency tests.

Models	$\Delta\lvert y \rvert$				
	90.0 kPa	75.0 kPa	60.0 kPa	45.0 kPa	30.0 kPa
NRTL	0.003	0.001	0.001	0.003	0.004
Wilson	0.002	0.001	0.001	0.002	0.002
UNIQUAC	0.008	0.008	0.008	0.008	0.008
Point to point test results	Passed	Passed	Passed	Passed	Passed

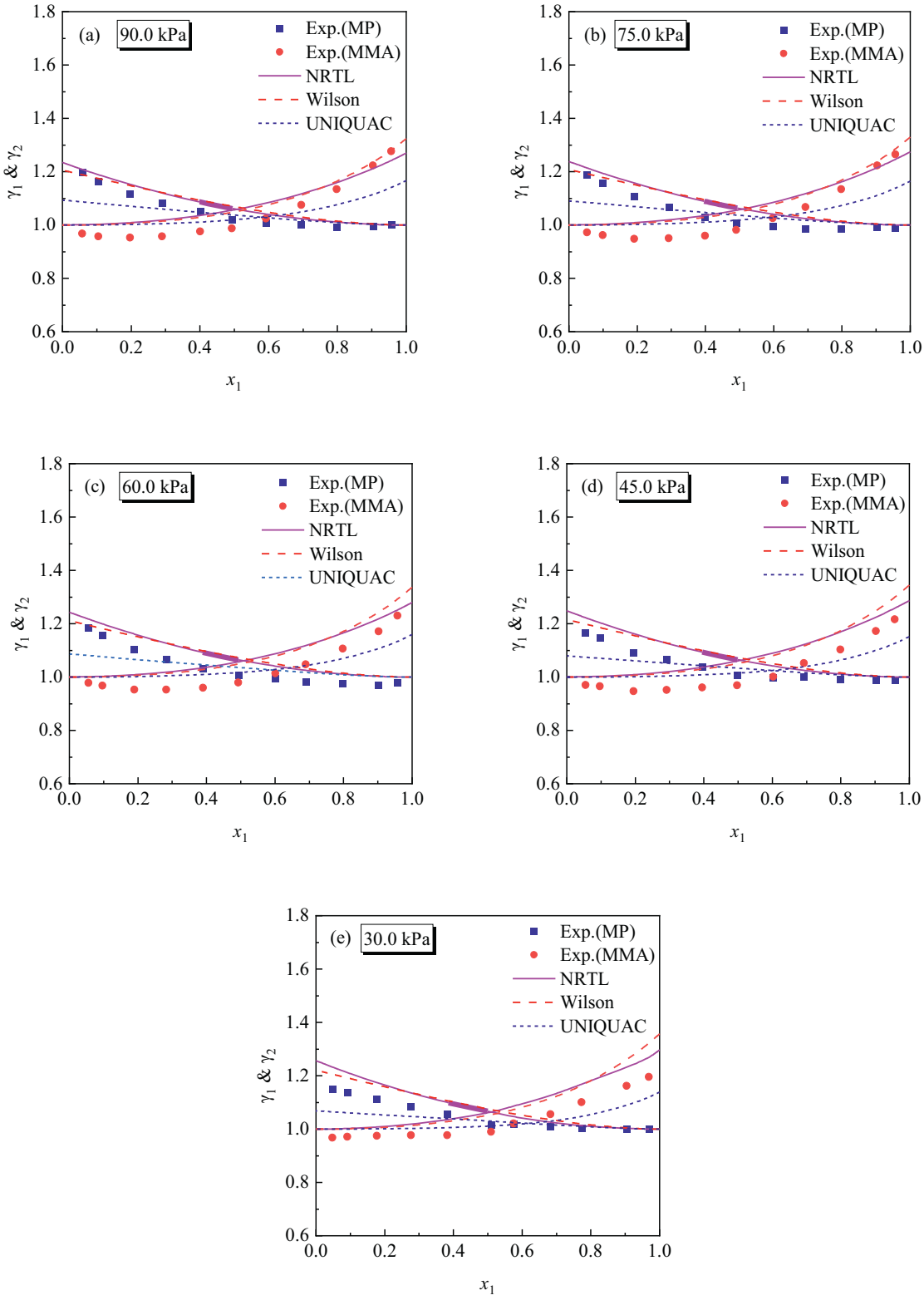

Fig. 5. Experimental and calculated values of γ_i for the binary system of MP–MMA at different pressures: (a) 90.0 kPa, (b) 75.0 kPa, (c) 60.0 kPa, (d) 45.0 kPa and (e) 30.0 kPa.

differences among the fitting models, the simulation model was established with flow rate of 100 kg·h^{-1}, the feed composition of MP 5% (mass) and MMA 95% (mass), which is aligned with industrial MMA production realities. The separation target of the simulation model requires MMA purity ≥99.9% (mass). The sensitivity analysis was conducted on the number of theoretical

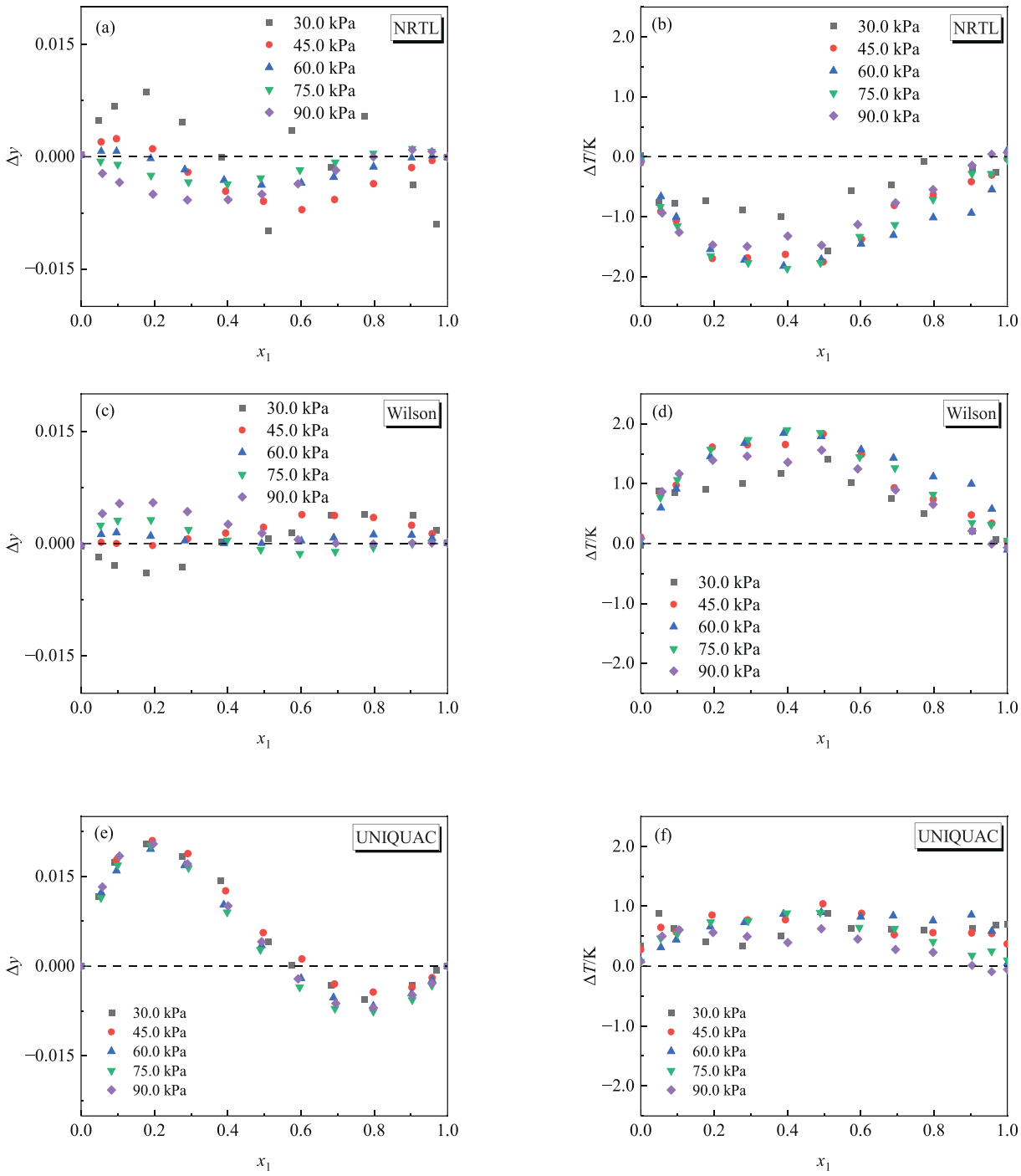

Fig. 6. Correlated data at equilibrium temperature (T) and vapor composition of MP (y_1) as a function of liquid composition of MP (x_1) with three models, where "◆" 90.0 kPa, "▼"75.0 kPa, "▲" 60.0 kPa, "●"45.0 kPa, "■" 30.0 kPa, (a) and (b) for NRTL, (c) and (d) for Wilson, (e) and (f) for UNIQUAC.

stages, feed stage and reflux ratio based on the obtained binary interaction parameters, and the results are shown in Fig. 7. The simulation results reveal that the UNIFAC model requires up to 49 stages, significantly more than other thermodynamic models evaluated. In contrast, the fitted models with regressed parameters, NRTL, Wilson, and UNIQUAC require significantly fewer stages, with 25, 26, and 27 stages, respectively. As shown in Fig. 7(b), the optimal feed positions of the models are basically located at 14th to 16th stages, while the feed stage up to 20 when using the NRTL model. According to the results illustrated in Fig. 7(c), the optimal reflux ratios for the Wilson and UNIQUAC models are the 17 and 20. The value is higher than the 15 obtained by the NRTL model and significantly lower than the 23 derived from the UNIFAC model with the same separation target. This indicates that the separation of MP–MMA is relatively easier compared to the group contribution estimation approach. The specific operation parameters and material balance for the separation of MP and MMA are obtained by using Aspen Plus

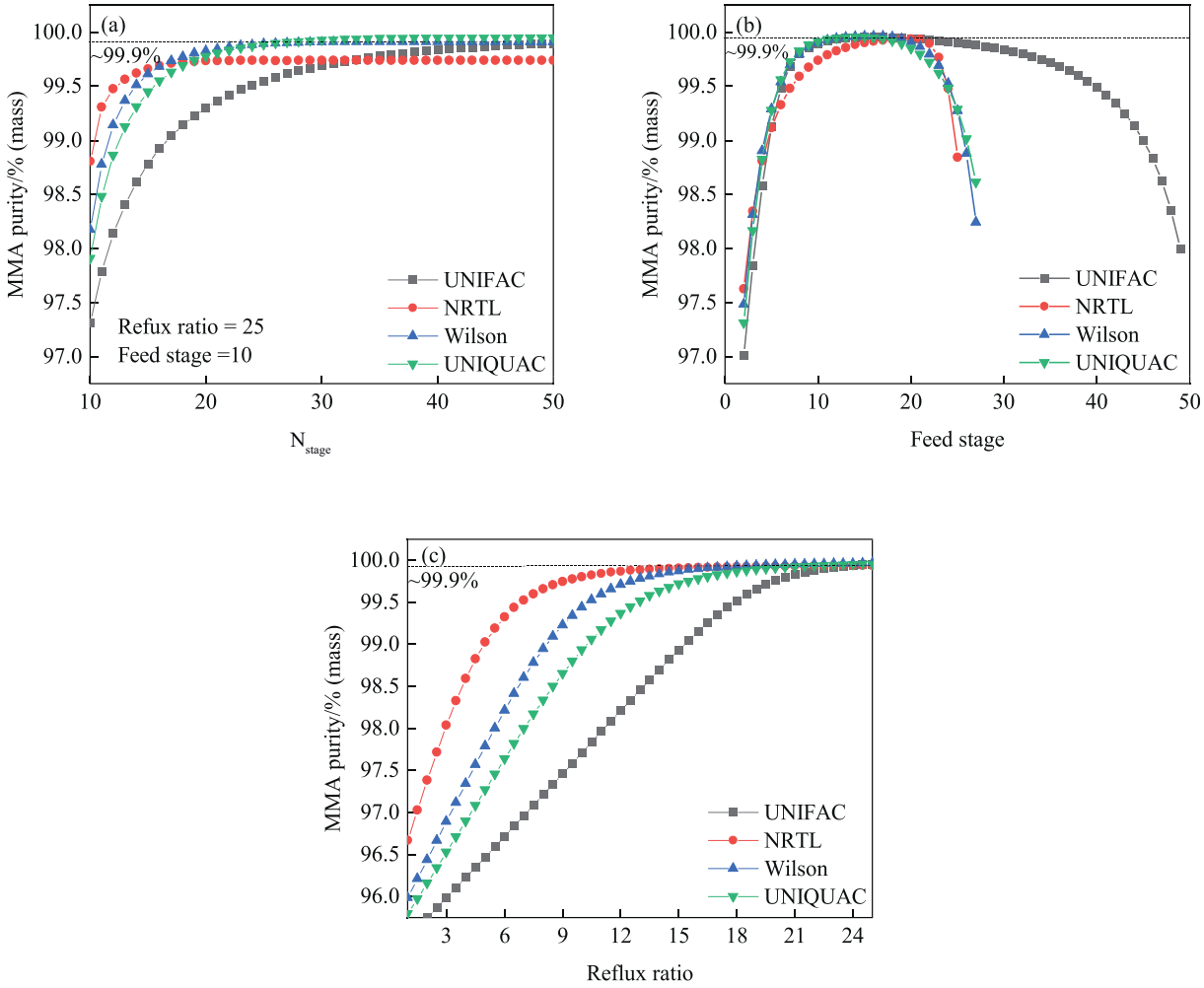

Fig. 7. Sensitivity analysis of the distillation tower: (a) number of stages, (b) feed stage and (c) reflux ratio.

and are shown in Table 9 and Tables S5–S8. These findings offer crucial support for engineering design and industrial applications. This reduction in the number of theoretical stages substantially lowers investment costs while still fulfilling the separation requirements.

To better demonstrate the effectiveness of the revised thermodynamic method in practical applications, an in-depth analysis and study on the estimation of equipment investment with parameters correction further conducted with the Eqs. (19)–(22) [37]. The total equipment investment costs mainly include the tower shell, tower tray and heat exchangers, the results have been listed in Table 9. The results show that the model with corrected parameters has a reduction of more than 38% in total equipment investment cost compared to the UNIFAC estimation model, indicating that the correction of VLE parameters has practical application value in guiding process design and production.

$$H = \frac{N}{0.85} \times 0.6096 \tag{19}$$

$$\text{Shell cost} = 22688.6 D^{1.066} H^{0.802} \tag{20}$$

$$\text{Tray cost} = 1426.0 D^{1.55} H \tag{21}$$

$$\text{Heat transfer cost} = 9367.8 \times \left(\frac{Q}{u \times \Delta T}\right)^{0.65} \tag{22}$$

where H (m) represents the tower height, N represents the number of trays, D (m) represents the tower diameter and calculated by Aspen Plus, Q (kW) represents the heat load of the condenser or reboiler, u ($kW \cdot K^{-1} \cdot m^{-2}$) represents the heat transfer coefficient, with the heat

Table 9
The operating parameters for separation of MP and MMA binary systems.

	UNIFAC	NRTL	Wilson	UNIQUAC
Pressure/kPa	50	50	50	50
Reflux ratio	23	15	17	20
Number of stages	49	25	26	27
Feed location	16	20	15	14
Temperature at the 1st stage/K	332.1	332.0	332.0	332.1
Temperature at the last stage/K	351.4	351.3	351.4	351.4
MMA mass fraction in top flow	0.016	0.015	0.016	0.017
MMA mass fraction in bottom flow	0.999	0.999	0.999	0.999
Yield of MMA product/% (mass)	99.9	99.9	99.9	99.9
Total investment costs/CNY	70338.3	35692.0	38705.2	43488.5
Cost savings ratio/%	/	49.3	45.0	38.2

transfer coefficient of the condenser being 0.852 $kW \cdot K^{-1} \cdot m^{-2}$ and that of the reboiler being 0.568 $kW \cdot K^{-1} \cdot m^{-2}$, ΔT (K) represents the heat exchange temperature difference.

4. Conclusions

The VLE data for the binary system composed of MP–MMA were successfully determined by a modified Rose equilibrium still at 90.0, 75.0, 60.0, 45.0, and 30.0 kPa. The reliability and consistency of the experimental data were validated using the Herington area test and the Fredenslund point test. The data passed both tests, thereby validating the precision of the experimental setup and methodology. Furthermore, a comprehensive correlation analysis of the experimental data using three activity coefficient models reveals that the RMSD and AAD values are in alignment, suggesting that the experimental data are highly consistent with NRTL and Wilson models. The results show that the relative volatility between MP and MMA increases as the pressure decreases, suggesting that lower pressure operations enhance the efficacy of the separation process. Finally, the interaction parameters derived from the regression analysis of the VLE can be effectively employed in the design and optimization of the MP–MMA separation process, the model with corrected parameters has a reduction of more than 38% in total equipment investment cost compared to the UNIFAC model, indicating that the correction of VLE parameters has practical application value in guiding process design and production, thus facilitating more efficient and cost-effective industrial applications.

CRediT Authorship Contribution Statement

Junping Zhang: Writing – original draft, Software, Data curation. Songsong Chen: Visualization, Validation, Funding acquisition, Data curation. Shasha Cao: Visualization, Software. Chunshan Li: Writing – review & editing, Formal analysis. Hui Zhao: Writing – review & editing, Project administration. Xiangping Zhang: Project administration, Funding acquisition, Conceptualization. Chaohe Yang: Supervision, Methodology, Conceptualization.

Declaration of Competing Interest

The authors declare that they have no known competing financial interests or personal relationships that could have appeared to influence the work reported in this paper.

Acknowledgements

This work was financially funded by National Key Research & Development Program of China (2022YFC3902200), Key Research & Development Program of Henan Province (241111230500), Strategic Priority Research Program of Chinese Academy of Sciences (Class A) (XDA29040500) and the National Natural Science Foundation of China (22578466).

Supplementary Material

Supplementary data to this article can be found online at https://doi.org/10.1016/j.cjche.2025.09.019.

References

[1] R.Y. Yan, Z.X. Li, Y.Y. Diao, C. Fu, H. Wang, C.S. Li, Q. Chen, X.P. Zhang, S.J. Zhang, Green process for methacrolein separation with ionic liquids in the production of methyl methacrylate, *AIChE J.* 57 (9) (2011) 2388–2396.
[2] B.A. Bhanvase, D.V. Pinjari, P.R. Gogate, S.H. Sonawane, A.B. Pandit, Synthesis of exfoliated poly(styrene-co-methyl methacrylate)/montmorillonite nanocomposite using ultrasound assisted *in situ* emulsion copolymerization, *Chem. Eng. J.* 181-182 (2012) 770–778.
[3] X.Y. Ji, D.Y. Chen, Y. Zheng, J.B. Shen, S.Y. Guo, E. Harkin-Jones, Multi-layered assembly of poly(vinylidene fluoride) and poly(methyl methacrylate) for achieving multi-shape memory effects, *Chem. Eng. J.* 362 (2019) 190–198.
[4] B. Wang, S.L. Deng, Y.H. Bian, G.L. Zhang, C.S. Li, Aldol condensation of methyl propionate and formaldehyde: thermodynamics, reaction process, and network, *Ind. Eng. Chem. Res.* 61 (43) (2022) 15910–15916.
[5] G. Wang, X.M. Hu, S.R. Zhao, Kinetic and thermodynamic studies on direct synthesis of methyl methacrylate from methyl propionate and methanol catalyzed by highly efficient cobalt complex at mild conditions, *Chem. Eng. J.* 468 (2023) 143592.
[6] Z.D. Young, S. Hanspal, R.J. Davis, Aldol condensation of acetaldehyde over titania, hydroxyapatite, and magnesia, *ACS Catal.* 6 (5) (2016) 3193–3202.
[7] P. Nising, T. Meyer, Modeling of the high-temperature polymerization of methyl methacrylate. 1. Review of existing models for the description of the gel effect, *Ind. Eng. Chem. Res.* 43 (23) (2004) 7220–7226.
[8] I. Pappas, R. Bindlish, M. Ali, E.N. Pistikopoulos, Optimal operation of an industrial dividing wall column through multiparametric programming, *Ind. Eng. Chem. Res.* 62 (37) (2023) 15029–15035.
[9] Y.H. Shi, H.Q. Wu, J.M. Xu, Studies on vapor–liquid equilibrium of binary systems containing the MMA component under normal atmospheric pressure, *J. Chem. Eng. Data* 67 (12) (2022) 3650–3660.
[10] J. Polak, B.C.Y. Lu, Vapor–liquid equilibriums of methyl propanoate–methanol and methyl propanoate–ethanol systems at 25.deg, *J. Chem. Eng. Data* 17 (4) (1972) 456–458.
[11] A. Shariati, L.J. Florusse, M.C. Kroon, C.J. Peters, Bubble point pressures of binary system of methanol and methyl propionate, *Fluid Phase Equilib.* 417 (2016) 166–170.
[12] Q.L. Lu, J.L. Li, C.J. Peng, H.L. Liu, Experimental determination of vapor liquid equilibrium for methanol + methyl propionate + 1-butyl-3-methylimidazolium bis(trifluoromethylsulfonyl)imide at atmospheric pressure, *J. Chem. Thermodyn.* 132 (2019) 289–294.
[13] T. Ishikawa, B.C.Y. Lu, Vapor–liquid equilibria of the methanol–methyl methacrylate system at 313.15, 323.15 and 333.15 K, *Fluid Phase Equilib.* 3 (1) (1979) 23–34.
[14] O. Redlich, A.T. Kister, Thermodynamics of nonelectrolyte solutions - *x–y–t* relations in a binary system, *Ind. Eng. Chem.* 40 (2) (1948) 341–345.
[15] T.F. Zhu, S. Yao, Z.D. Wang, W. Liu, H. Song, Isobaric vapor–liquid equilibria for the binary and ternary systems of 2-methyl-1-butanol, 2-methyl-butanol acetate, and dimethylformamide (DMF) at 101.3 kPa, *J. Chem. Eng. Data* 58 (5) (2013) 1156–1160.
[16] J. Wisniak, J. Ortega, L. Fernández, A fresh look at the thermodynamic consistency of vapour–liquid equilibria data, *J. Chem. Thermodyn.* 105 (2017) 385–395.
[17] R.D. Chirico, M. Frenkel, J.W. Magee, V. Diky, C.D. Muzny, A.F. Kazakov, K. Kroenlein, I. Abdulagatov, G.R. Hardin, W.E. Acree Jr., J.F. Brenneke, P.L. Brown, P.T. Cummings, T.W. de Loos, D.G. Friend, A.R.H. Goodwin, L.D. Hansen, W.M. Haynes, N. Koga, A. Mandelis, K.N. Marsh, P.M. Mathias, C. McCabe, J.P. O'Connell, A. Pádua, V. Rives, C. Schick, J.P.M. Trusler, S. Vyazovkin, R.D. Weir, J. T. Wu, Improvement of quality in publication of experimental thermophysical property data: challenges, assessment tools, global implementation, and online support, *J. Chem. Eng. Data* 58 (10) (2013) 2699–2716.
[18] M.T. Zafarani-Moattar, N. Tohidifar, Vapor–liquid equilibria, density, and speed of sound for the system poly(ethylene glycol) 400 + methanol at different temperatures, *J. Chem. Eng. Data* 51 (5) (2006) 1769–1774.
[19] R. Ríos, J. Ortega, L. Fernández, I. de Nuez, J. Wisniak, Improvements in the experimentation and the representation of thermodynamic properties (*iso-p* VLE and yE) of alkyl propanoate + alkane binaries, *J. Chem. Eng. Data* 59 (1) (2014) 125–142.
[20] W. Fan, Q. Zhou, J. Sun, S.J. Zhang, Density, excess molar volume, and viscosity for the methyl methacrylate + 1-butyl-3-methylimidazolium hexafluorophosphate ionic liquid binary system at atmospheric pressure, *J. Chem. Eng. Data* 54 (8) (2009) 2307–2311.
[21] C.T. Hsieh, M.J. Lee, H.M. Lin, Vapor–liquid–liquid equilibria for aqueous systems with methyl acetate, methyl propionate, and methanol, *Ind. Eng. Chem. Res.* 47 (20) (2008) 7927–7933.
[22] J.T. Chen, Y.M. Lin, Liquid–liquid equilibria for the ternary systems water + 1-propanol + methyl methacrylate, +butyl methacrylate, and +isobutyl methacrylate, *Fluid Phase Equilib.* 258 (1) (2007) 1–6.
[23] S.S. Chen, L. Dong, J.P. Zhang, W.G. Cheng, F. Huo, Q. Su, W. Hua, Effects of imidazolium-based ionic liquids on the isobaric vapor–liquid equilibria of methanol + dimethyl carbonate azeotropic systems, *Chin. J. Chem. Eng.* 28 (3) (2020) 766–776.
[24] L.Y. Wang, H. Zhao, L.J. Han, Y.F. Wang, J.Y. Xin, Isobaric vapor–liquid equilibrium of binary mixtures of 2-methylpentanedioic acid dimethyl ester and dimethyl adipate at 101.3, 50.0, 30.0, and 10.0 kPa, *J. Chem. Eng. Data* 69 (4) (2024) 1613–1620.
[25] F. Li, T. Zhang, L. Lv, W.X. Tang, Y. Wang, S.W. Tang, Effects of ionic liquids on the vapor–liquid equilibriumof 1,3,5-trioxane–water system at 101.3 kPa, *Chin. J. Chem. Eng.* 73 (2024) 42–50.
[26] J. Ortega, F. Espiau, M. Postigo, Excess properties and isobaric vapor–liquid equilibria for binary mixtures of methyl esters + *tert*-butanol, *J. Chem. Eng. Data* 49 (6) (2004) 1602–1612.

[27] W.V. Steele, R.D. Chirico, A.B. Cowell, S.E. Knipmeyer, A. Nguyen, Thermodynamic properties and ideal-gas enthalpies of formation for trans-methyl cinnamate, α-methyl cinnamaldehyde, methyl methacrylate, 1-nonyne, trimethylacetic acid, trimethylacetic anhydride, and ethyl trimethyl acetate, *J. Chem. Eng. Data* 47 (4) (2002) 700–714.
[28] C.C. Du, Z.P. Du, B.W. Long, H.M. Du, Z.G. Yan, X. Yin, Isobaric vapor–liquid equilibria of binary mixtures of diethyl carbonate with methyl acetate, *n*-propyl acetate, or amyl acetate at 100.17 kPa, *J. Chem. Eng. Data* 64 (6) (2019) 2550–2557.
[29] K. Yue, G.W. Zhou, Isobaric vapor–liquid equilibrium for ethyl acetate + ethanol with ionic liquids [MMIM][DMP] and [OMIM][PF6] as entrainers, *J. Mol. Liq.* 348 (2022) 118404.
[30] X.C. Yang, H.X. Li, C.M. Cao, Z.P. Zou, L. Xu, G.J. Liu, Isobaric vapor–liquid equilibrium for the binary system of dimethyl adipate and 1,6-hexanediol at 10, 20, and 99 kPa, *J. Chem. Eng. Data* 64 (10) (2019) 4256–4263.
[31] C.C. Zuo, Y.P. Li, C.S. Li, S.S. Cao, H.Y. Yao, S.J. Zhang, Thermodynamics and separation process for quaternary acrylic systems, *AIChE J.* 62 (1) (2016) 228–240.
[32] G.M. Wilson, Vapor–liquid equilibrium. XI. A new expression for the excess free energy of mixing, *J. Am. Chem. Soc.* 86 (2) (1964) 127–130.
[33] D.S. Abrams, J.M. Prausnitz, Statistical thermodynamics of liquid mixtures: a new expression for the excess Gibbs energy of partly or completely miscible systems, *AIChE J.* 21 (1) (1975) 116–128.
[34] H.L. Chen, L. Zhang, Y.L. Huang, J.J. Lu, Z.J. Zhao, X.Q. Wang, Isobaric vapor–liquid equilibrium of three binary systems containing dimethyl succinate, dimethyl glutarate and dimethyl adipate at 2, 5.2 and 8.3 kPa, *J. Chem. Thermodyn.* 133 (2019) 100–110.
[35] J.I. Carrero-Mantilla, D. de Jesus Ramírez-Ramírez, J.F. Súarez-Cifuentes, Thermodynamic and statistical consistency of vapor–liquid equilibrium data, *Fluid Phase Equilib.* 412 (2016) 158–167.
[36] C.H. Xing, Y.Y. Wu, B. Wu, K. Chen, L.J. Ji, Vapor–liquid equilibrium for the binary systems involving cumene, *t*-butylbenzene, and *sec*-butylbenzene at 101.3 kPa, *J. Chem. Eng. Data* 69 (3) (2024) 1026–1033.
[37] Z.X. Zhou, Y.D. Guo, S.S. Chen, G.J. Cui, A.L. Bao, F. Huo, J.P. Zhang, A new multi-objective optimization algorithm for separation processes, *Chem. Eng. Res. Des.* 213 (2025) 159–171.